Climate warming has led to the degradation of permafrost stability in the past half century over the Qinghai-Tibet Plateau

Youhua Ran[1,2], Xin Li[1,2,3], Guodong Cheng[1,4]

[1]Key Laboratory of Remote Sensing of Gansu Province, Heihe Remote Sensing Experimental Research Station, Cold and
5 Arid Regions Environmental and Engineering Research Institute, Chinese Academy of Sciences, Lanzhou 730000, China
[2]University of Chinese Academy of Sciences, Beijing 100049, China
[3]CAS Center for Excellence in Tibetan Plateau Earth Sciences, Beijing 100101, China
[4]Institute of Urban Studies, Shanghai Normal University, Shanghai, Shanghai 200234, China

Correspondence to: Xin Li (lixin@lzb.ac.cn)

10 **Abstract.** Temperature increases cause a unique type of damage to permafrost. This damage is often expressed as the degradation of permafrost thermal stability, which is very important for engineering design, resource development, and environmental protection in cold regions. This study evaluates the degradation of permafrost stability over the QTP from the 1960s to the 2000s using estimated decadal mean annual air temperatures (MAATs) by integrating remote sensing-based estimates of mean annual land surface temperatures (MASTs), leaf area index (LAI) and fractional snow cover values, and
15 decadal mean MAATs taken at 152 weather stations using geographically weighted regression (GWR). The results reflect a continuous rise of approximately 0.04 ℃/a in the decadal mean MAAT values over the past half century. Climate warming has led to a reduction in permafrost stability in the past half century. The total degraded area of stability is approximately 153.76×10^4 km^2, which corresponds to 87.98% of the permafrost area in the 1960s. The stability of 75.24% of the extremely stable permafrost, 89.56% of the stable permafrost, 90.3% of the sub-stable permafrost, 92.31% of the transitional
20 permafrost, and 32.8% of the unstable permafrost has been reduced to lower levels of stability. Approximately 49.4% of the unstable permafrost and 95.95% of the extremely unstable permafrost has degraded to seasonally frozen ground. The sensitivity of the permafrost to climate is dependent on its stability level. The mean elevations of the extremely stable, stable, sub-stable, transitional, unstable, and extremely unstable permafrost areas increased by 88 m, 97 m, 155 m, 185 m, 161 m and 250 m, respectively. The degradation mainly occurred from the 1960s to the 1970s and from the 1990s to the 2000s.
25 This degradation has led to increases in risks to infrastructure, increased flood risks, reductions in ecosystem resilience, and positive climate feedback effects. It therefore affects the well-being of millions of people and sustainable development at the Third Pole.

1 Introduction

Permafrost is defined as soil or rock that includes ice or organic material and remains at or below 0 ℃ for at least two years
30 (Permafrost Subcommittee, National Research Council of Canada. 1988; Williams et al., 1989). Temperature rise causes a

unique type of dynamic damage to permafrost (Zhu et al., 2016). This damage is often expressed as the degradation of permafrost thermal stability, which is very important for engineering design, construction, resource development, the carbon and water cycles and ecological protection in cold regions (Collett, 2002; Cheng and Wu, 2007; Tarnocai et al, 2009; Schuur et al, 2009; Schaefer et al, 2011; Hinzman et al., 2013; Mu et al., 2015).

5   In terms of middle- and high-altitude permafrost regions, the area of permafrost in China is the largest in the world, as the Qinghai-Tibet Plateau (QTP) permafrost experiences higher temperatures than those seen in Siberia and the Arctic, which are more sensitive to global climate warming and human activity (Wu et al., 2002; Haeberli and Hohmann, 2008; Li et al., 2008; Ran et al., 2012; Ran and Li, 2016). On the QTP, mean annual air temperature (MAAT) increased by approximately 0.2~0.4 ℃ from the 1970s to the late 1990s (Wang et al., 2000). From 1961–2010, the decadal average MAAT rose by 1.3 ℃,

10 with an average rate of increase of 0.03 ℃/a (Jin et al., 2011; Ran and Li, 2016). Correspondingly, significant permafrost degradation is occurring. From 1996 to 2001, the thickness of the active layer increased by 0.15~0.50 metres, and the mean annual ground temperature (MAGT) rose by 0.1–0.5 ℃ in the past 30 years (Yang et al., 2010). At Xidatan, which is near the city of Golmud and at the northern boundary of the permafrost on the QTP along the Qinghai-Tibet Railway (QTR), the lower limit of permafrost moved upward by approximately 25 m from 1975 through 2002 (Nan et al., 2003). The lower limit

15 of permafrost on the northern and southern slopes of the Bayan Har Mountains, where a region of discontinuous permafrost occurs in the southern part of Qinghai province, moved upward by approximately 100 metres and 90 metres, respectively, from 1991 to 2010 (Luo et al., 2012). During 2006 to 2012, on the southern side of the Tanggula Mountains permafrost region along the QTR, both the engineered structures and ongoing climate change caused the permafrost degradation to accelerate. The permafrost table declined by 0.29 m and 0.41 m, and the ground temperature at a depth of 10 m rose by 0.03℃

20 and 0.06℃, respectively, within areas of undisturbed permafrost and the permafrost under the embankment (Sun et al., 2014). Cheng et al. (2012) reported on the decadal changes in permafrost distribution on the QTP over the past 50 years (1960–2009) and demonstrated that the rate of permafrost loss had accelerated since the 1980s, and about one-fifth of the total area of permafrost that existed in the 1960s has degraded.

  However, many of these studies focus on either the local or in situ scales, and few studies have focused on the regional scale.

25 Although the decadal changes in the permafrost distribution over the QTP were simulated by Cheng et al. (2012), this study emphasized the migration of permafrost "boundaries" based on the relationship between air temperature and the lower limit of the permafrost. Naturally, these boundaries are continuous, inexact representations of the permafrost distribution and permafrost degradation (Yang et al., 2010). Ran and Li (2016) assessed the degradation of permafrost stability in China over the past 30 years; however, this study used a near-surface air temperature reanalysis dataset with low resolution and large

30 uncertainties. These studies are not comprehensive and do not adequately reflect changes in the thermal state of the permafrost, especially in the interior of permafrost zones and at high spatial resolution. More importantly, the response time and the depth to which permafrost is affected by climate warming depend on the extents, durations, amplitudes, and rates of climate warming and are closely related to soil types, surface coverage, ice content, groundwater occurrence, geothermal anomalies, and human activities (Cheng and Jin, 2013). The complex physical mechanisms of the interactions between

climate change and permafrost are currently poorly understood (Jin et al., 2011), and a large of degree of uncertainty may exist in their evaluations. The current warming climate may not cause large areas of permafrost to disappear, because the thermal inertia of permafrost may allow it to persist for a long time (Cheng et al., 2012). Therefore, the utility of assessing changes in permafrost "boundaries" is limited in specific applications, especially in the field of engineering (Cheng, 1984;

5   Harris, 1986; Wu et al., 2002; Ran and Li, 2016).

Additionally, regional-scale evaluations usually rely on meteorological data. The most commonly used variable is air temperature, but measurements of this quantity are sparse on the Qinghai-Tibetan Plateau. Although the sparse air temperature measurements are interpolated onto grids based on digital elevation models (DEMs), the uncertainty of the gridded air temperatures is significant because of the heterogeneity of the surface characteristics, including snow cover and

10   vegetation, and the locations of weather stations (Vancutsem et al., 2010). Fortunately, the remote sensing era has led to changes in this situation. Thermal infrared remote sensing provides direct observations of land surface temperatures (LSTs) at high spatial and temporal resolutions. For example, the Moderate Resolution Imaging Spectroradiometer (MODIS) LST product is freely available and has been validated over large areas via a series of field campaigns. Its accuracy is better than 1 K (0.5 K in most cases) (Wan et al, 2002; 2004; 2008). Remote sensing-based estimates of LSTs provide a key high-

15   resolution temperature pattern of the land surface that can potentially be used in monitoring of permafrost degradation. However, criteria for using LST estimates to distinguish permafrost types are not traditionally available, and the relatively short time series of LST data does not meet the needs of long-term permafrost monitoring. Therefore, the remote sensing-based LST values must be converted to MAATs, which are commonly used in mapping permafrost. Several previous studies have demonstrated the potential of satellite-based methods in estimating near-surface air temperatures (Hachem et al., 2009;

20   2012; Vancutsem et al., 2010; Yao and Zhang, 2013). The variation in the uncertainty is mainly related to the underlying surface type, the amount of solar radiation, and cloud cover (Vancutsem et al., 2010; Hachem et al., 2012; Ran et al., 2015). Snow, which has high albedo in the visible and near-infrared bands and high emissivity in the thermal inferred band, a high absorption rate in the infrared and thermal infrared band, high heat capacity, and low thermal conductivity, influences the thermal shift in LSTs and air temperatures. This influence varies with the time of snowfall, snow accumulation, snow depth

25   and snow density (Henderson-Sellers and Hughes, 1982; Zhang, 2005). Vegetation is another important factor that affects the thermal shift of LSTs and air temperatures. This process is very complex. In general, the extinction effect of vegetation cover will reduce the amount of solar radiation reaching the ground surface. The vegetation canopy affects the water and heat balance of the soil-atmosphere system by intercepting rainfall and transpiring water. The vegetation fraction, vegetation height and vegetation type are important input parameters in the vegetation parameterizations used in land surface models

30   (Lawrence et al., 2011). However, it is more important that highly accurate remote sensing-based snow cover and vegetation products are also available. All of these remote sensing-based data products are very important for estimating the MAAT, which is an air temperature index used in monitoring the thermal stability of permafrost.

Therefore, the objective of this study is to evaluate the degradation of permafrost stability over the QTP during the past 50 years using a thermal stability classification system, multi-criterion remote sensing observations and an air temperature

observation network. The paper is organized as follows. In this section, we describe the gaps in the evaluation of permafrost degradation in previous studies and the objective of the paper. In section 2, the permafrost classification system and the methodology and data used in this paper are described. Section 3 presents the results and analyses the characteristics of permafrost stability degradation. In section 4, we summarize the paper and conclude.

2 Methods and Datasets

2.1 Permafrost thermal stability classification system

We use the thermal stability permafrost classification system proposed by Cheng (1984). Using this system, permafrost is classified into extremely stable, stable, sub-stable, transitional, unstable, and extremely unstable types, as shown in Table 1. Obviously, it is more useful to describe permafrost degradation from an engineering perspective, rather than changes in the extent of permafrost. Three criteria, the MAGT, the permafrost thickness, and the MAAT, were used to assess the stability types. The MAGT is the most direct indicator of the thermal state of permafrost. However, long-term measurements of the MAGT are almost impossible, due to the high cost of drilling boreholes. The MAAT is frequently used in mapping the distribution of permafrost. It is easy to measure and has high spatial representativeness. Importantly, long-term in situ measurements of MAATs are available, and it is possible to estimate MAATs over the QTP using remote sensing-based methods, as introduced in the section above. The MAAT is therefore used in this paper. On the QTP, a MAAT of −2℃ has typically been used to distinguish permafrost from seasonally frozen ground (Cheng, 1984; Ran and Li, 2016). However, the extremely unstable type in the Cheng classification system refers to regions that include cave ice and frozen gravel below the lower limit of permafrost. In this paper, a MAAT of −1℃ is used to distinguish extremely unstable permafrost from seasonally frozen ground.

2.2 Simulation of MAAT using geographically weighted regression

In this study, geographically weighted regression (GWR) is used to simulate MAATs. Local parameters are employed in the GWR model to estimate MAATs while considering the spatial locations of meteorological stations (Brunsdon et al., 1998; Kumar et al., 2012). The weighting is a function of the distance between the location of each regression point and the sites where observations are available. The GWR model used in the present study is shown below in Equation (1):

$$y_i = \beta_0(\mu_i, \upsilon_i) + \sum_{k=1}^{m} \beta_k(\mu_i, \upsilon_i) x_{ik} + \varepsilon_i \tag{1}$$

where y_i is the MAAT at pixel i, x_{ik} is the kth explanatory factor at pixel i, $\beta_0(\mu_i, \upsilon_i)$ and $\beta_k(\mu_i, \upsilon_i)$ represent the intercept and slope for the kth explanatory factor, m is the number of explanatory factors, and ε_i is the residual term.

The quantities $\beta_0(\mu_i, \upsilon_i)$ and $\beta_k(\mu_i, \upsilon_i)$ are estimated using Equation (2):

$$\hat{\beta}(\mu_i, \upsilon_i) = (X^T W(\mu_i, \upsilon_i)X)^{-1} X^T W(\mu_i, \upsilon_i)Y \qquad (2)$$

where $\hat{\beta}(\mu_i, \upsilon_i)$ is an unbiased estimation of the regression coefficients. It is a vector that include an intercept and m regression coefficients associated with m explanatory factors. X is a matrix of explanatory factors ($n \times m$); $W(\mu_i, \upsilon_i)$ is the spatial weight matrix, which is a diagonal matrix; Y is a vector ($n \times 1$) for the dependent variables, i.e., the decadal mean MAAT; and n is the number of MAAT observation stations.

In this study, the Gaussian function is used as a spatial weighting function, as shown in Equation (3):

$$W(\mu_i, \upsilon_i) = \exp\left(-\frac{1}{2}\left(\frac{d_i}{r}\right)^2\right) \qquad (3)$$

where d_i is the distance between the ith observation station and the point to be estimated, and r is the bandwidth parameter. To accommodate different station densities, the corrected Akaike information criterion (AICc) is used to determine the optimal bandwidth parameters.

A stepwise linear regression analysis is used to select the independent variables for the GWR model. As shown in Table 2, the analysis shows that the use of the MAST, the leaf area index (LAI), the fractional snow cover (FSC), altitude, latitude, and longitude as independent variables (i.e., Model 6) results in the highest degree of explanatory power. The variance inflation factor (VIF) was used to assess the multicollinearity of the model. A VIF value <1.5 shows that the degree of tolerance is high, and the multicollinearity of the model is thus acceptable. We assume that the pattern of vegetation, snow cover, and LST are consistent over the past 50 years. The GWR model is then used to estimate the decadal mean MAAT over the QTP in the past 50 years. The SAGA (System for Automated Geoscientific Analyses) (Conrad et al., 2015) is used to implement the GWR.

2.3 Evaluation of the degradation of permafrost thermal stability

The following linear regression model is used to evaluate the warming rate or degradation rate over the QTP in the past 50 years.

$$Y = a + bx + \varepsilon \qquad (4)$$

where Y denotes the MAAT or permafrost area, x is the time, ε is the error, a is the intercept, and b is the slope (i.e., the warming rate or the degradation rate). The statistical significance of the warming rates or degradation rate is evaluated using Student's *t*-test.

Thirteen altitude ranges (<3600 m, 3600-3800 m, 3800-4000 m, 4000-4200 m, 4200-4400 m, 4400-4600 m, 4600-4800 m, 4800-5000 m, 5000-5200 m, 5200-5400 m, 5400-5600 m, 5600-5800 m, and >5800 m) are used to evaluate the altitude

dependence of the warming rate. The degradation of permafrost thermal stability is evaluated from two perspectives, the change in area of the different thermal stability types and the spatial heterogeneity of the change. For the area change, we calculate the total area of each thermal stability type during the past five decades and the rate of change (i.e., the degradation rate) using the linear regression model shown in Equation (4). The spatial pattern of the degradation of permafrost thermal

5 stability is evaluated at two levels. At the pixel level, the spatial distribution of the degradation is evaluated. At the level of the thermal stability types, a transfer matrix is used to evaluate the conversions among the thermal stability types (Stehman, 1997). We also analyse the changes in the altitude histograms for each thermal stability type in the past 50 years.

2.4 Datasets

2.4.1 Mean annual land surface temperature

10 MODIS Terra/Aqua daytime and nighttime LST products (MOD11A1 and MYD11A1, version 5) with a spatial resolution of 1 km and covering 2006 to 2010 were acquired from the Distributed Active Archive Center (DAAC) operated by the U.S. National Aeronautics and Space Administration (NASA). These data are used in this study to estimate MASTs. A pragmatic approach proposed by Ran et al., (2015) and Ran et al., (2017) was employed to estimate the MASTs using the four daily MODIS LST products. This approach assumes that the arithmetic average of the daytime and nighttime LSTs represent the

15 daily mean LST with acceptable accuracy, and the daily amplitude of LST is more homogeneous than the LST itself (Liu et al., 2006; Kogan et al., 2011; Ran et al., 2015). The approach allows the full use of every value at any time in any pixel of the MODIS LST products through the use of the temporally and spatially complete LST daily amplitude, which is interpolated using a gap filling algorithm (Garcia, 2010). This algorithm employs a penalized least squares regression based on discrete cosine transforms that explicitly utilizes information from a time series to predict the missing values. The

20 penalized least squares regression is a thin-plate spline smoother for a generally one-dimensional data array, and it can trade off fidelity to the data versus the roughness of the mean function (Garcia, 2010; Wang, et al., 2012). This approach is easy to implement and independent of other observations. Validation shows that the scheme is effective in restore the missing values in MODIS instantaneous LST observations and produce a spatially and temporally continuous daily average LST dataset that displays good agreement with observations made at the ground surface. The errors in the result originate mainly from the

25 original instantaneous LST MODIS products. A more detailed description of this scheme can be found in Ran et al., (2015) and Ran et al., (2017).

The temporally and spatially continuous daily mean LSTs from January 1, 2006 to December 31, 2010 and the corresponding MASTs used in this study are produced using the above approach.

2.4.2 Fractional snow cover

30 Arithmetic mean values of daily cloud-removed FSC products from 2006 to 2010 are used in this study. This product is derived from the daily MODIS 500-m snow cover product (MOD10A1) using a gap filling process based on a cubic spline

interpolation algorithm. A comparison with reference FSC Sr data obtained from Landsat ETM+ shows the high accuracy with which this product reflects snow cover information over the QTP (Tang et al., 2013). The cloud-removed FSC products were acquired from the Cold and Arid Regions Science Data Center at Lanzhou in China (http://westdc.westgis.ac.cn).

2.4.3 Leaf area index

5 Annual mean LAI values obtained from the Global Land Surface Satellite (GLASS), which make up a high quality LAI product with an eight-day temporal resolution and a 1-km spatial resolution and cover the period from 2006 to 2010, were used in this study. The GLASS LAI product is derived from the fused MODIS and CYCLOPES LAI products, and the remaining effects of cloud contamination have been removed using MODIS time series surface reflectance data and general regression neural networks (Xiao et al., 2014). The results of validation show that the GLASS LAI product has a lower

10 uncertainty than the MODIS and CYCLOPES LAI products (Xiang et al., 2014). The GLASS LAI product was acquired from the GLASS project website (http://glass-product.bnu.edu.cn/en).

2.4.4 In situ MAAT observations

The MAAT measurements, which were collected at 152 stations from 1960 to 2010 within the QTP and the surrounding area, were acquired from the data centre of the China Meteorological Administration (http://cdc.nmic.cn). The distribution of

15 these stations is shown in Figure 1. The decadal mean MAAT values over the past 50 years are used in this study.

2.4.5 Validation data

Validation of the long-term stability of permafrost is difficult due to the limited amounts of reference data that are available. In this study, we evaluate the results by comparing the estimated permafrost distribution in the 2000s with previous regional-scale permafrost maps and borehole measurements at individual sites. The permafrost maps that cover the QTP from Li and

20 Cheng, (1996), Nan et al. (2002), and Zou et al., (2016) are used at the regional scale. In particular, the map of Zou et al., (2016) integrates the MODIS eight-day LST product within the framework of the temperature at the top of the permafrost (TTOP) model (Smith and Riseborough, 1996), and careful validation of this map has been performed using MAGT data. At the site scale, the MAGT values used in this study were collected from 142 boreholes presented in the existing literature (Yu et al., 2008; Wang et al., 2013; Luo et al., 2013) and the International Permafrost Association (IPA)-International Polar Year

25 (IPY) Thermal State of Permafrost (TSP) Snapshot Borehole Inventory downloaded from the National Snow and Ice Data Center (NSIDC) (http://nsidc.org) (International Permafrost Association, 2010). The distribution of these boreholes is shown in Figure 1.

2.4.6 Ancillary data

The distribution of water bodies in the MODIS land cover product (MOD12Q1) and the map showing the distribution of

30 glacier ice from the second Chinese glacier inventory are used to support the permafrost area statistics. The MOD12Q1

product is used for consistency with the other remote sensing products employed in this study. On the other hand, the glacier extents from the second Chinese glacier inventory are compiled based on Landsat TM/ETM+ images acquired from 2004 to 2011, as well as other ancillary data, such as digital elevation models (DEMs). The robust band ratio segmentation method is first used to delineate the glacier outlines, and intensive manual improvements are then performed to improve its accuracy.

5 An error assessment shows that the area error for all of the glaciers in China is approximately 3.2% (Guo et al., 2015).

3 Results and Discussion

Decadal mean MAAT estimates with a resolution of 1 km over the QTP in the past 50 years are produced using the GWR model. The mean coefficient of determination of this model is approximately 0.95. The permafrost stability map in the past five decades is then produced based on the simulated MAAT and the permafrost stability types defined in Table 1.

10 ### 3.1 Change of MAAT over the QTP in the past 50 years

The MAATs over the QTP have risen continuously in the past 50 years. The mean MAAT values for the 1960s, 1970s, 1980s, 1990s, and 2000s are -2.38°C, -1.85°C, -1.78°C, -1.32°C, and -0.58°C, respectively. These values reflect a continuous rise with a rate of approximately 0.04°C/a. This value is higher than the global average warming rate, as well as the estimated warming rates for the QTP reported by Cheng et al. (2012) and Ran et al. (2016) that are based on interpolated

15 altitude-based air temperature data or surface air temperature reanalysis data. The warming rate in the western part of the QTP is higher than that in the eastern part and depends on altitude, as shown in Figure 2 and Figure 3. The warming rate increases with increasing altitude from approximately 0.33°C per decade at 3600 m to 0.49°C per decade at 5200 m. This finding is similar to that of previous studies (Liu and Chen, 2000; Qin et al., 2009). The physical mechanisms of this phenomenon may be related to the combined effects of the cloud-radiation and snow-albedo feedbacks (Giorgi et al., 1997;

20 Liu et al., 2009). These elevated warming rates may have a substantial impact on the thermal stability of the permafrost.

3.2 Thermal stability degradation

Based on the map of permafrost stability types covering the past five decades (Figure 4a-e), we analyse the degradation from three perspectives, including temporal changes, spatial changes in the map plane, and spatial changes with altitude.

3.2.1 Temporal dynamics of thermal stability

25 The permafrost thermal stability has degraded continuously over the past 50 years. The area occupied by the stable types has decreased continuously, and the area occupied by the unstable types has increased continuously (Table 3). The areas occupied by the extremely stable, stable, sub-stable, and transitional types display net decreases of approximately 8.99×10^4 km^2 (72.79%), 27.06×10^4 km^2 (70.12%), 9.30×10^4 km^2 (27.24%), and 1.18×10^4 km^2 (4.77%) from the 1960s to the 2000s, respectively. In particular, the stable type displays the most serious degradation, and its rate of loss is approximately

6.15×10^4 km^2 (15.94%) per decade. Moreover, the area occupied by the unstable type has increased by approximately 3.99×10^4 km^2 (9.02%) at a rate of 1.06×10^4 km^2 (2.4%) per decade. Specifically, this degradation mainly occurred during the 1960s to 1970s and the 1980s to 1990s for the extremely stable type, the 1960s to the 1970s and the 1990s to the 2000s for the stable type, and the 1980s to the 2000s for the sub-stable type. The area occupied by the extremely unstable type has not

5 changed substantially. Overall, the warming climate has caused a degradation of permafrost stability. If glaciers and the extremely unstable type are included, the total area of the permafrost region has decreased significantly from 174.76×10^4 km^2 in the 1960s to 133.1×10^4 km^2 in the 2000s at a rate of approximately 9.52×10^4 km^2 (5.45%) per decade, and this loss of area occurred mainly during the 1960s to the 1970s and the 1990s to the 2000s (Table 3).

3.2.2 Spatial changes in thermal stability

10 The degradation of thermal stability has occurred over a broad region of permafrost on the QTP within the past 50 years, especially during the 1960s to the 1970s and the 1990s to the 2000s. The degradation of permafrost stability in the western QTP was serious during the 1960s to the 1970s. In the subsequent 40 years, the degradation of permafrost stability in the QTP was relatively homogeneous (Figure 4f-i). Specifically, the extents of the extremely stable, stable, and sub-stable types retreated from the south to the north (Figure 4a-e). The extents of the transitional, unstable, and extremely unstable types

15 extended northward correspondingly. Approximately 42.30% of the area occupied by the extremely stable type, 42.09% of the area occupied by the stable type, and 39.83% of the area occupied by the sub-stable type have degraded to the stable, sub-stable, and transitional types from the 1960s to the 1970s, respectively. At the same time, approximately 57.26% of the area occupied by the transitional type, 29.34% of the area occupied by the unstable type, and 59.47% of the area occupied by the extremely unstable type, have degraded to the unstable type, the extremely unstable type, and seasonally frozen ground,

20 respectively. Overall, approximately 75.24% of the area occupied by the extremely stable type, 89.56% of the area occupied by the stable type, 90.3% of the area occupied by the sub-stable type, 92.31% of the area occupied by the transitional type, and 32.8% of the area occupied by the unstable type have degraded to lower levels of stability in the past 50 years (Table 4). The reduction in the area occupied by the permafrost is mainly due to the degradation of the area occupied by the unstable and extremely unstable types. Approximately 49.4% of the area occupied by the unstable type and 95.95% of the area

25 occupied by the extremely unstable type has degraded to seasonally frozen ground (Table 4). The total degraded area is approximately 153.76×10^4 km^2, which accounts for 87.98% of the area occupied by the permafrost region in the 1960s (Figure 4j). The area of permafrost for which the stability has not changed is approximately 21×10^4 km^2 (12.02%). This area is mainly distributed in the central part of the plateau, which contains extremely high mountains, and it is dominated by the extremely stable type.

30 It should be noted that the stability of an area of permafrost of approximately 1.63×10^4 km^2 has increased. This area is found primarily east of Lhasa in the southeastern part of the QTP, which is a major centre of marine glaciers and snow cover in China (Figure 4j). The increased permafrost stability in this area may have large uncertainties; the uncertain MAAT trend is

estimated using regression parameters that are appropriate for low-altitude areas, due to the lack of long-term MAAT measurements in the high mountain regions where glaciers and snow are prevalent. In snow-dominated regions, the MAAT trend cannot simply be used to infer changes in permafrost stability because the ground temperature is independent of the MAAT (Stieglitz et al., 2003; Lawrence et al., 2008). The effects of snow or glacier cover may be more important than those of the MAAT. Although records of long-term snow cover and glacier changes in the past 50 years are not available in this study, the sensitivity of glacier and snow cover in a warming climate is dependent on the area of the glaciers and the climate zone. Low snow–climate sensitivities have been found in continental interior climates with relatively cold and dry winters (Brown and Mote, 2009). Larger glaciers have lower climate sensitivities (Ding and Haeberli, 1996; Ye et al., 2001). Therefore, we believe the permafrost stability in this area has not changed substantially in the past 50 years, based on this low climate sensitivity.

3.2.3 Altitude changes in permafrost stability type distribution

The altitude statistics of the distribution of the permafrost stability types over the QTP in the past five decades indicate that the altitude occupied by each permafrost stability type in the QTP has risen continuously (Table 5, Figure 5). For the extremely stable type, the mean altitude of the distribution decreased from 5240 m to 5161 m from the 1960s to the 1970s and then rose continuously at a rate of approximately 56.4 m per decade. The reduction in altitude is mainly due to the degradation of the extremely stable permafrost type in the Kailas Mountains. As a whole, in the past 50 years, the mean rate of rise of the extremely stable type has been approximately 24.7 m per decade. Moreover, the mean altitudes of the stable, sub-stable, transitional, unstable, and extremely unstable types have risen at a rate of 23.6 m, 36.3 m, 43 m, 36.5 m, and 56.2 m, respectively. Overall, the mean altitudes of the extremely stable, stable, sub-stable, transitional, unstable, and extremely unstable types increased by 88 m, 97 m, 155 m, 185 m, 161 m, and 250 m in the past 50 years. This result indicates that the climate sensitivity of permafrost is dependent on the stability level. The extremely unstable permafrost type is the most sensitive of the permafrost types to climate warming. As in the last section, the degradation mainly occurred from the 1960s to the 1970s and from the 1990s to the 2000s.

3.3 Discussion

3.3.1 Cross validation and uncertainty analysis

We validate the permafrost extent only in the 2000s because long-term records of permafrost stability and extent are not available in earlier periods, as mentioned in section 2.4.5. Comparison of the estimated permafrost extent in the 2000s with the permafrost map provided by Zou et al., (2016) shows that the difference is small. Within permafrost areas, the extremely unstable type of permafrost mainly refers to cave ice and frozen gravel, which are distributed below the lower limit of permafrost (Cheng, 1984). This kind of permafrost is usually not counted in the total area of permafrost. Therefore, the permafrost area in the 2000s is approximately 107.19×10^4 km^2 if glaciers and lakes are neglected. This result is closely

similar to that of Zou et al., (2016), who showed that the permafrost area in the 2000s was approximately $106.47 \times 10^4 \, \text{km}^2$. The permafrost distribution is also very similar to that presented by Zou et al., (2016) (Figure 6). The consistency between the two distributions is 92%, and the kappa coefficient is approximately 0.82. At the site scale, 89% of the 142 locations are consistent with the borehole survey, whereas this proportion is only 74%, 28%, and 86% for the maps of Li and Cheng, (1996), Nan et al. (2002), and Zou et al. (2016), respectively. These proportions indicate that the accuracy of the permafrost extent identified in this study is at least comparable with that of Zou et al. (2016).

The uncertainty of the results may result primarily from the thermal inertia of deep soil layers in cold regions, errors in the geothermal flux, insufficient resolution, inaccuracies in the surface station data, or the sparseness of these stations, which are especially sparse in high mountain areas. First, the low heat conductivity of soil leads to lags between increases in surface temperatures and the subsequent increases in permafrost temperature or reductions in permafrost thickness (Li et al., 1996). The delay time is longer for permafrost thickness than temperature and varies with the thermal stability type (Li et al., 1996; Wu et al., 2010). For the stable type, the degradation of permafrost may be delayed by "thermal offset" and "seasonal offset" effects in the permafrost table due to the negative heat budget; i.e., the amount of heat released from the active layer during the winter is greater than the amount of heat absorbed in summer (Smith and Riseborough, 2002; Wu et al., 2010). For the unstable type, a positive heat budget appears in the upper soil layer that leads to a greater degradation rate than that seen in stable permafrost, since the thickness of the unstable type is smaller than that of the stable type (Li et al., 1996; Wu et al., 2010). Second, the thawing of the base of the permafrost induced by the geothermal heat flux leads to the permafrost degrading from bottom to top (Jin et al., 2006; Wu et al., 2010). The missing geothermal heat flux may lead to a delay in permafrost degradation, especially for the stable permafrost, because the geothermal flux is independent of air temperature. Third, although the resolution of the simulation has been significantly improved to 1 km, it is still coarse relative to the degradation rate of mountain permafrost. Its degradation is presented in terms of the increase in the elevation of the lower limit of the permafrost, which is generally about a hundred metres. On the other hand, a 1 km change in the horizontal extent change may correspond to a change in altitude of hundreds of metres. Last, the lack of long-term MAAT measurements in the glacier and snow dominated high mountain regions may lead to errors in the estimated MAATs.

3.3.2 The implications of the degradation of thermal stability

The degradation of permafrost stability in the QTP has important impacts on the safety of infrastructure in the permafrost regions, water quality, ecosystem health, and the feedbacks on regional and global climates. First, as the permafrost stability degrades, the risk of deterioration and damage to engineered structures in permafrost zones will increase. This indicates that the measures used to prevent permafrost degradation may need to be enhanced for new structures. For example, permafrost accounted for 90.1% of a 10-km-long segment of the QTR from Golmud to Lhasa in the 1960s, and these permafrost areas were dominated by the sub-stable type; however, after 50 years (i.e., in the 2000s), these permafrost areas accounted for only 67.77% and were dominated by the unstable type. For "warm" permafrost areas that are dominated by unstable permafrost, an enhanced measure to prevent permafrost degradation, i.e., the proactive roadbed cooling approach, has been successfully

applied in constructing the QTR (Cheng, 2004; 2005; Cheng et al., 2008). Second, the degradation of permafrost in the QTP may affect the hydrologic cycle in the Third Pole region, which includes the QTP and the surrounding arid regions. Permafrost controls the distribution, recharge, flow paths, discharge, dynamics, and hydrochemistry of groundwater (Cheng and Jin, 2013). The degradation of permafrost affects the interactions among the surface water, subsoil water, and

5 groundwater by changing the hydraulic conductivity and hydraulic connectivity of the soil. The degradation of the ice-rich permafrost itself makes important contributions to surface runoff and the development of thermokarst lakes in the inner Tibetan Plateau (Zhang et al., 2013). The enhanced drainage may lead to increases in flood risk (Larsen et al., 2008) and reductions in ecosystem resilience via seasonal shifts in stream flow and groundwater abundance, because the decrease in permafrost water storage capacity in the QTP will lead to a reduction in dry-season water availability. All of these changes

10 will affect the well-being of millions of people and sustainable development at the Third Pole, which contains the headwater areas of several of the major rivers in Southeast Asia, such as the Yellow, Yangtze, Mekong, Yarlung Zangbo and Shiquan Rivers. The Third Pole also includes many inland rivers, such as the Shiyang, Heihe, Shule, and Tarim Rivers, in northwestern China. Last, the permafrost region in the QTP contains approximately 160 Pg of organic carbon (Mu et al., 2015) and many thermokarst lakes and wetlands (Niu et al., 2011; Luo et al., 2015). Thawing of the permafrost may lead to

15 the disappearance or growth of thermokarst lakes (Smith et al., 2005), which may further affect greenhouse gas emissions and produce a feedback effect on climate change (Tarnocai et al., 2009; Schuur et al. 2009; Schaefer et al., 2011; McCalley et al., 2014). Additionally, changes in thermokarst lakes may both accelerate and delay permafrost thawing (Westermann et al., 2016; You et al., 2017).

4 Conclusions

20 This study evaluates the stability degradation of permafrost over the QTP from the 1960s to the 2000s based on the estimated decadal means of the mean annual air temperatures (MAATs) over the Qinghai-Tibet Plateau (QTP) in the past 50 years obtained by integrating remote sensing-based mean annual land surface temperatures (MASTs), leaf area index (LAI) and fractional snow cover values, and decadal mean MAATs measured at 152 weather stations using a geographically weighted regression (GWR) model. Cross validation shows that the accuracy of the estimated permafrost extent is greater than that of

25 previous maps.

The decadal mean MAATs reflect a continuous rise at a rate of approximately 0.04 ℃/a during the past half century. The warming rate increases with increasing altitude from approximately 0.33°C per decade at 3600 m to 0.49°C per decade at 5200 m and then decreases as altitude increases further. Climate warming has led to the degradation of permafrost stability in the past half century. The area occupied by the stable permafrost types has continuously decreased, and the area occupied by

30 the unstable permafrost types has continuously increased. The total degraded area is approximately 153.76×10^4 km^2, which accounts for 87.98% of the permafrost area in the 1960s. The stability of 75.24% of the area occupied by the extremely stable type, 89.56% of the area occupied by the stable type, 90.3% of the area occupied by the sub-stable type, 92.31% of the

area occupied by the transitional type, and 32.8% of the area occupied by the unstable type have degraded to lower levels. The extent of the extremely stable, stable, and sub-stable types retreated from the south to the north, whereas the extent of the transitional, unstable, and extremely unstable types extended northward. The mean elevations of the extremely stable, stable, sub-stable, transitional, unstable, and extremely unstable types increased by 88 m, 97 m, 155 m, 185 m, 161 m and 250 m, respectively. This result indicates that the climate sensitivity of permafrost is dependent on the stability level. The degradation mainly occurred during two periods that include the 1960s to the 1970s and the 1990s to the 2000s. The degradation of permafrost stability in the QTP has important impacts on the safety of infrastructure, flood risks, ecosystem resilience, and climate feedbacks, as well as the well-being of millions of people and sustainable development at the Third Pole.

However, the uncertainties inherent in this analysis cannot be discounted. These uncertainties are due to asynchronous changes in near-surface air temperatures and deep soil layer temperatures, the missing geothermal flux, insufficient resolution, or the inaccuracies and sparseness of the surface station data employed. As this evaluation is empirically based, obtaining more convincing results requires additional data, especially from the deep layers of soils. The development of new, fast, and inexpensive sensors and robust machine learning methods will assist in this effort. A physically based definition of permafrost stability and an improved physically based model will contribute to the prediction of permafrost stability degradation and its interactions with the engineering stability of infrastructure, the water cycle, and climate change.

Acknowledgements:

References

Brown, R. D. and Mote, P. W.: The response of Northern Hemisphere snow cover to a changing climate. Journal of Climate, 22(8), 2124-2145, 2009.

Brunsdon, C., Fotheringham, S., and Charlton, M.: Geographically weighted regression. Journal of the Royal Statistical Society: Series D (The Statistician), 47(3), 431-443, 1998.

Cheng, G. D.: Problems on zonation of high-altitude permafrost. ACTA Geographica Sinica, 39,185–193, 1984. (in Chinese)

Cheng, G.: Influences of local factors on permafrost occurrence and their implications for Qinghai-Xizang Railway design. Science in China Series D: Earth Sciences, 47(8), 704-709, 2004.

Cheng, G.: A roadbed cooling approach for the construction of Qinghai–Tibet Railway. Cold regions science and technology, 42(2), 169-176, 2005.

Cheng, G. D. and Wu, T. H.: Responses of permafrost to climate change and their environmental significance, Qinghai-Tibet Plateau. Journal of Geophysical Research, 112, F02S03, doi: 10.1029/2006JF000631, 2007.

Cheng, G., Sun, Z., and Niu, F.: Application of the roadbed cooling approach in Qinghai–Tibet railway engineering. Cold regions science and technology, 53(3), 241-258, 2008.

Cheng, W.M., Zhao, S.M., Zhou, C.H., and Chen, X.: Simulation of the Decadal Permafrost Distribution on the Qinghai-Tibet Plateau (China) over the Past 50 Years. Permafrost and Periglacial Processes, 23(4), 292–300, 2012.

Cheng, G.D. and Jin, H.J.: Permafrost and groundwater on the Qinghai-Tibet Plateau and in northeast China. Hydrogeology Journal, 21(1), 5–23, 2013.

Collett, T. S.: Energy resource potential of natural gas hydrates. AAPG bulletin, 86(11), 1971-1992, 2002.

Conrad, O., Bechtel, B., Bock, M., Dietrich, H., Fischer, E., Gerlitz, L., Wehberg, J., Wichmann, V., and Böhner, J.: System for automated geoscientific analyses (SAGA) v. 2.1. 4. Geoscientific Model Development, 8(7), 1991-2007, 2015.

Ding, Y. and Haeberli, W.: Compilation of long-term glacier-fluctuation data in China and a comparison with corresponding records from Switzerland. Journal of glaciology, 42(141), 389-400, 1996.

Garcia, D.: Robust smoothing of gridded data in one and higher dimensions with missing values. Computational Statistics & Data Analysis, 54, 1167-1178, 2010.

Giorgi, F., Hurrell, J. W., Marinucci, M. R., and Beniston, M.: Elevation dependency of the surface climate change signal: a model study. Journal of Climate, 10(2), 288-296, 1997.

Guo, W., Liu, S., Xu, J., Wu, L., Shangguan, D., Yao, X., Wei, J., Bao, W., Yu, P., Liu, Q., and Jiang, Z.: The second Chinese glacier inventory: data, methods and results. Journal of Glaciology, 61(226), 357-372, 2015.

Hachem, S., Allard, M., and Duguay, C.: Using the MODIS land surface temperature product for mapping permafrost: an application to Northern Quebec and Labrador, Canada. Permafrost and Periglacial Processes, 20(4), 407-416, 2009.

Hachem, S., Duguay, C. R., and Allard, M.: Comparison of MODIS-derived land surface temperatures with near-surface soil and air temperature measurements in continuous permafrost terrain. The Cryosphere, 6, 51-69, 2012.

Haeberli, W. and Hohmann, R.: Climate, glaciers and permafrost in the Swiss Alps 2050: scenarios, consequences and recommendations. In: Kane DL, Hinkel KM (Eds.). Proceedings Ninth International Conference on Permafrost, vol.1. Institute of Northern Engineering, University of Alaska Fairbanks, pp. 607–612, 2008.

Haeberli, W. and Hohmann, R.: Climate, glaciers and permafrost in the Swiss Alps 2050: scenarios, consequences and recommendations. In Proceedings Ninth International Conference on Permafrost, 1, 607-612, 2008.

Harris, S. A.: Permafrost distribution, zonation and stability along the eastern ranges of the Cordillera of North America. Arctic, 29-38, 1986.

Henderson-Sellers, A. and Hughes, N. A.: Albedo and its importance in climate theory. Progress in Physical Geography, 6(1), 1-44, 1982.

Hinzman, L. D., Deal, C. J., McGuire, A. D., Mernild, S. H., Polyakov, I. V., and Walsh, J. E.: Trajectory of the Arctic as an integrated system. Ecological Applications, 23(8), 1837-1868, 2013.

International Permafrost Association (IPA).: IPA-IPY Thermal State of Permafrost (TSP) Snapshot Borehole Inventory, Version 1. Boulder, Colorado USA. NSIDC: National Snow and Ice Data Center. doi: 10.7265/N57D2S25, 2010.

Jin, H., Luo, D., Wang, S., Lü, L., and Wu, J.: Spatiotemporal variability of permafrost degradation on the Qinghai-Tibet Plateau. Sciences in Cold and Arid Regions, 3(4), 281-305, 2011.

Jin, H., Zhao, L., Wang, S., and Jin, R.: Thermal regimes and degradation modes of permafrost along the Qinghai-Tibet Highway. Science in China Series D: Earth Sciences, 49(11), 1170-1183, 2006.

Jorgenson, M. T., Romanovsky, V., Harden, J., Shur, Y., O'Donnell, J., Schuur, E. A., Kanevskiy, M., and Marchenko, S.: Resilience and vulnerability of permafrost to climate change. Canadian Journal of Forest Research, 40(7), 1219-1236, 2010.

Kogan, F., Powell, A., and Fedorov, O.: Use of Satellite and In-Situ Data to Improve Sustainability. Springer, 2011.

Kumar, S., Lal, R., and Liu, D.: A geographically weighted regression kriging approach for mapping soil organic carbon stock. Geoderma, 189, 627-634, 2012.

Lawrence, D. M., Slater, A. G., Romanovsky, V. E., and Nicolsky, D. J.: Sensitivity of a model projection of near-surface permafrost degradation to soil column depth and representation of soil organic matter. Journal of Geophysical Research: Earth Surface, 113(F2), 2008.

Lawrence, D. M., Oleson, K. W., Flanner, M. G., Thornton, P. E., Swenson, S. C., Lawrence, P. J., Zeng X.B., Yang Z. L., Levis, S., Sakaguchi, K., Bonan, G. B., and Slater, A. G.: Parameterization improvements and functional and structural advances in version 4 of the Community Land Model. Journal of Advances in Modeling Earth Systems, 3(1), 2011.

Larsen, P. H., Goldsmith, S., Smith, O., Wilson, M. L., Strzepek, K., Chinowsky, P., and Saylor, B.: Estimating future costs for Alaska public infrastructure at risk from climate change. Global Environmental Change,18(3), 442-457, 2008.

Li, X., Cheng, G., Jin, H., Kang, E., Che, T., Jin, R., Wu, L., Nan, Z.T., Wang, J., and Shen, Y.: Cryospheric change in China. Global and Planetary Change, 62(3), 210-218, 2008.

Li, S. D. and Cheng, G.D.: Map of permafrost on the Qinghai-Tibet Plateau (1:3,000,000). Gansu Culture Press: Lanzhou, 1996. (in Chinese).

Li, S., Cheng, G., and Guo, D.: The future thermal regime of numerical simulating permafrost on Qinghai-Xizang (Tibet) Plateau, China, under climate warming. Science in China Series D-earth Sciences, 39(4), 434-441, 1996.

Lin, Z., Niu, F., Xu, Z., Xu, J., and Wang, P.: Thermal regime of a thermokarst lake and its influence on permafrost, Beiluhe Basin, Qinghai-Tibet Plateau. Permafrost and Periglacial Processes, 21(4), 315-324, 2010.

Liu, X. and Chen, B.: Climatic warming in the Tibetan Plateau during recent decades. International journal of climatology, 20(14), 1729-1742, 2000.

Liu, X. D., Yin, Z.Y., Shao, X. M., and Qin, N. S.: Temporal trends and variability of daily maximum and minimum, extreme temperature events, and growing season length over the eastern and central Tibetan Plateau during 1961–2003. Journal of Geophysical Research, 111(D19109), doi:10.1029/2005JD006915, 2006.

Liu, X., Cheng, Z., Yan, L., and Yin, Z. Y.: Elevation dependency of recent and future minimum surface air temperature trends in the Tibetan Plateau and its surroundings. Global and Planetary Change, 68(3), 164-174, 2009.

Luo, D. L., Jin, H. J., Lin, L., You, Y. H., Yang, S. Z., and Wang, Y. P.: Distributive features and controlling factors of permafrost and the active layer thickness in the Bayan Har Mountains along the Qinghai-Kangding Highway on Northeastern Qinghai-Tibet Plateau. Scient Geograph Sin, 33, 635-640, 2013. (In Chinese, English abstract)

Luo, J., Niu, F., Lin, Z., Liu, M., and Yin, G.: Thermokarst lake changes between 1969 and 2010 in the beilu river basin, qinghai–tibet plateau, China.Science Bulletin, 60(5), 556-564, 2015.

McCalley, C. K., Woodcroft, B. J., Hodgkins, S. B., Wehr, R. A., Kim, E. H., Mondav, R., Crill, P.M., Chanton, J. P., Rich, V.I., Tyson, G.W., and Saleska, S. R.: Methane dynamics regulated by microbial community response to permafrost thaw. Nature, 514(7523), 478-481, 2014.

Mu, C., Zhang, T., Wu, Q., Peng, X., Cao, B., Zhang, X., and Cheng, G.: Editorial: Organic carbon pools in permafrost regions on the Qinghai–Xizang (Tibetan) Plateau. The Cryosphere, 9(2), 479-486, 2015.

Nan, Z. T., Li, S. X., and Liu, Y, Z.: Mean annual ground temperature distribution on the Tibetan Plateau: Permafrost distribution mapping and further application. Journal of Glaciology and Geocryology, 24(2), 142-148, 2002. (in Chinese)

Nan, Z., Gao, Z., Li, S., and Wu, T.: Permafrost changes in the northern limit of permafrost on the Qinghai-Tibet Plateau in the last 30 years. Acta Geographica Sinica, 58(6): 817–823, 2003. (In Chinese, English abstract)

Niu, F., Lin, Z., Liu, H., and Lu, J.: Characteristics of thermokarst lakes and their influence on permafrost in Qinghai–Tibet Plateau. Geomorphology,132(3), 222-233, 2011.

Permafrost Subcommittee, National Research Council of Canada.: Glossary of Permafrost and Related Ground-ice Terms. National Research Council of Canada Technical Memorandum, 1988.

Qin, J., Yang, K., Liang, S., and Guo, X.: The altitudinal dependence of recent rapid warming over the Tibetan Plateau. Climatic Change, 97, 321-327, 2009.

Ran, Y., Li, X., Cheng, G., Zhang, T., Wu, Q., Jin, H., and Jin, R.: Distribution of permafrost in China: an overview of existing permafrost maps. Permafrost and Periglacial Processes, 23(4), 322-333, 2012.

Ran, Y., Li, X., Jin, R., and Guo, J.: Remote sensing of the mean annual surface temperature and surface frost number for mapping permafrost in China. Arctic, Antarctic, and Alpine Research, 47(2), 255-265, 2015.

Ran, Y. H. and Li, X.: Evaluation of the permafrost stability degradation from 1980 to 2010 in China. Sciences in Cold and Arid Regions, 8(5), 0359–0366, doi: 10.3724/SP.J.1226.2016.00359, 2016.

Ran, Y.H., Li, X., and Cheng, G.D.: A permafrost thermal stability map over third pole by integrated remotely sensed land surface temperature, leaf area index, soil properties, and ground boreholes measurement. Submitted to Remote Sensing of Environment, 2017.

Schaefer, K., Zhang, T., Bruhwiler, L., and Barrett, A. P.: Amount and timing of permafrost carbon release in response to climate warming. Tellus B, 63(2), 165-180, 2011.

Schuur, E. A., Vogel, J. G., Crummer, K. G., Lee, H., Sickman, J. O., and Osterkamp, T. E.: The effect of permafrost thaw on old carbon release and net carbon exchange from tundra. Nature, 459(7246), 556-559, 2009.

Smith, M. W. and Riseborough, D. W.: Permafrost monitoring and detection of climate change. Permafrost and Periglacial Processes, 7(4), 301-309, 1996.

5   Smith, M. W., and Riseborough, D. W.: Climate and the limits of permafrost: a zonal analysis. Permafrost Periglacial Process, 13, 1-15, 2002.

Smith, L. C., Sheng, Y., MacDonald, G. M., and Hinzman, L. D. Disappearing arctic lakes. Science, 308(5727), 1429-1429, 2005.

Sun, Z. Z., Wu, G. L., Yun, H. B., Liu, G. J., and Rui, P. F.: Permafrost degradation under an embankment of the Qinghai-
10   Tibet Railway in the southern limit of permafrost. Journal of Glaciology and Geocryology, 36(4), 767-771, doi: 10.7522/j.issn.1000-0240.2014.0092, 2014. (In Chinese, English abstract)

Stehman, S. V.: Selecting and interpreting measures of thematic classification accuracy. Remote sensing of Environment, 62(1), 77-89, 1997.

Stieglitz, M., Déry, S. J., Romanovsky, V. E., and Osterkamp, T. E.: The role of snow cover in the warming of arctic
15   permafrost. Geophysical Research Letters, 30(13), 2003.

Tang, Z., Wang, J., Li, H., and Yan, L.: Spatiotemporal changes of snow cover over the Tibetan plateau based on cloud-removed moderate resolution imaging spectroradiometer fractional snow cover product from 2001 to 2011. Journal of Applied Remote Sensing, 7(1), 073582-073582, 2013.

Tarnocai, C., Canadell, J. G., Schuur, E. A. G., Kuhry, P., Mazhitova, G., and Zimov, S.: Soil organic carbon pools in the
20   northern circumpolar permafrost region. Global biogeochemical cycles, 23(2), 2009.

Vancutsem, C., Ceccato, P., Dinku, T., & Connor, S. J.: Evaluation of MODIS land surface temperature data to estimate air temperature in different ecosystems over Africa. Remote Sensing of Environment, 114(2), 449-465, 2010.

Wan, Z., Zhang, Y., Zhang, Q., and Li, Z.L.: Validation of the land-surface temperature products retrieved from Terra Mode rate Resolution Imaging Spectroradiometer data. Remote Sensing of Environment, 83, 163-180, 2002.

25   Wan, Z., Zhang, Y., Zhang, Q., and Li, Z.L.: Quality assessment and validation of the MODIS global land surface temperature. International Journal of Remote Sensing, 25, 261-274, 2004.

Wan, Z.: New refinements and validation of the MODIS land-surface temperature/emissivity products. Remote Sensing of Environment, 112(1): 59-74, 2008.

Wang, S.L., Jin, H.J., Li, S.X., and Zhao, L.: Permafrost degradation on the Qinghai-Xizang (Tibet) Plateau and its
30   environmental impacts. Permafrost and Periglacial Processes, 11, 43–53, 2000.

Wang, G., Garcia, D., Liu, Y., de Jeu, R., and Dolman, A.J.: A three dimensional gap filling method for large geophysical datasets: application to global satellite soil moisture observations. Environmental Modelling & Software, 30, 139-142, 2012.

Wang, Q. F., Zhang, T. J., Wu, J. C., Peng, X. Q., Zhong, X. Y., Mou, C., ... & Cheng, G. D.: Investigation on permafrost distribution over the upper reaches of the Heihe River in the Qilian Mountains. Journal of Glaciology and Geocryology, 35(1), 19-25, 2013. (In Chinese, English abstract)

Williams, P. J. and Smith, M.W.: The frozen earth: fundamentals of geocryology. UK, Cambridge: Cambridge University
5   Press, 1989.

Wu, Q.B., Zhu, Y.L., and Liu, Y.Z.: Evaluation model of permafrost thermal stability and thawing sensibility under engineering activity. Cold Regions Science and Technology, 34(1), 19–30, 2002.

Wu, J., Sheng, Y., Wu, Q., and Wen, Z.: Processes and modes of permafrost degradation on the Qinghai-Tibet Plateau. Science China Earth Sciences, 53(1), 150-158, 2010.

10   Xiang, Y., Xiao, Z. Q., Ling, S. L., Wang, J. D., and Song, J. L.: Validation of Global LAnd Surface Satellite (GLASS) leaf area index product. J. Remote Sens, 18, 573-596, 2014.

Xiao, Z., Liang, S., Wang, J., Chen, P., Yin, X., Zhang, L., and Song, J.: Use of general regression neural networks for generating the GLASS leaf area index product from time-series MODIS surface reflectance. IEEE Transactions on Geoscience and Remote Sensing, 52(1), 209-223, 2014.

15   Yang, M., Nelson, F. E., Shiklomanov, N. I., Guo, D., and Wan, G.: Permafrost degradation and its environmental effects on the Tibetan Plateau: A review of recent research. Earth-Science Reviews, 103(1), 31-44, 2010.

Yao, Y. and Zhang, B.: MODIS-based estimation of air temperature of the Tibetan Plateau. Journal of Geographical Sciences, 23(4), 627-640, 2013.

Ye, B. S., Ding, Y. J., and Liu, C. H.: Response of Valley Glaciers in Various Size and Their Runoff to Climate
20   Change. Journal of Glaciolgy and Geocryology, 23(2), 103-110, 2001. (In Chinese, English abstract)

Yoshikawa, K., and Hinzman, L. D.: Shrinking thermokarst ponds and groundwater dynamics in discontinuous permafrost near Council, Alaska. Permafrost and Periglacial Processes, 14(2), 151-160, 2003.

You, Y., Yu, Q., Pan, X., Wang, X., Guo, L., and Wu, Q. Thermal effects of lateral supra-permafrost water flow around a thermokarst lake on the Qinghai-Tibet Plateau. Hydrological Processes, 1-9, 2017.

25   Westermann, S., Langer, M., Boike, J., Heikenfeld, M., Peter, M., Etzelmüller, B., and Krinner, G. Simulating the thermal regime and thaw processes of ice-rich permafrost ground with the land-surface model CryoGrid 3. Geoscientific Model Development, 9, 523-546, 2016.

Yu, H., Wu, Q. B., and Liu, Y. Z.: The long-term monitoring system on permafrost regions along the Qinghai-Tibet Railway. Journal of Glaciology and Geocryology, 30(3), 475-481, 2008. (In Chinese, English abstract)

30   Zhang, T.: Influence of the seasonal snow cover on the ground thermal regime: An overview. Reviews of Geophysics, 43(4), 2005.

Zhang, G., Yao, T., Xie, H., Kang, S., and Lei, Y.: Increased mass over the Tibetan Plateau: from lakes or glaciers?. Geophysical Research Letters, 40(10), 2125-2130, 2013.

Zhu, Z., Kang, G., Ma, Y., Xie, Q., Zhang, D., and Ning, J.: Temperature damage and constitutive model of frozen soil under dynamic loading. Mechanics of Materials, 102, 108-116, 2016.

Zou, D., Zhao, L., Sheng, Y., Chen, J., Hu, G., Wu, T., Wu, J., Xie, C., Wu, X., Pang, Q., Wang, W., Du, E., Li, W., Liu, G., Li J., Qiu, Y., Qiao, Y., Wang, W., Shi, J., and Cheng, G.: A New Map of the Permafrost Distribution on the Tibetan

5   Plateau. The Cryosphere Discuss., doi:10.5194/tc-2016-187, 2016.

Table 1. Classification system used to assess permafrost stability (Cheng, 1984)

Type	Mean annual ground temperature (℃)	Thickness of permafrost (m)	Mean annual air temperature (℃)
Extremely stable	<-5.0	170	<-8.5
Stable	-3.0~-5.0	110~170	-6.5~-8.5
Sub-stable	-1.5~-3.0	60~110	-5.0~-6.5
Transitional	-0.5~-1.5	30~60	-4.0~-5.0
Unstable	+0.5~-0.5	0~30	-2.0~-4.0
Extremely unstable	>+0.5		-1.0>-2.0

Table 2. The statistics of the stepwise linear regression analysis

Model	Independent variables	Adjusted R^2	Significance level
1	MAST	0.83	0.00
2	MAST, LAI	0.87	0.00
3	MAST, LAI, FSC	0.88	0.00
4	MAST, LAI, FSC, Altitude	0. 90	0.00
5	MAST, LAI, FSC, Altitude, Longitude	0.91	0.00
6	MAST, LAI, FSC, Altitude, Longitude, Latitude	0.93	0.00

Table 3. The area statistics of the permafrost thermal stability types over the QTP in the past 50 years ($\times 10^4$ km^2)

Permafrost stability	1960s	1970s	1980s	1990s	2000s	2000s except for glaciers	Change rate ($\times 10^4$ km^2/decade)
Extremely stable	12.35	8.56	8.74	5.66	3.36	1.86	-2.09
Stable	38.59	28.30	27.64	20.91	11.53	10.39	-6.15
Sub-stable	34.14	34.75	34.09	31.94	24.84	24.03	-2.14
Transitional	24.73	23.95	23.59	23.39	23.55	23.12	-0.29
Unstable	44.22	43.89	43.70	46.51	48.21	47.80	1.06
Extremely unstable	20.73	21.05	20.54	20.16	21.63	21.56	0.09
Total area	174.76	160.50	158.32	148.57	133.10	128.76	-9.52

The Cryosphere
Discussions

Table 4. Transfer matrix of permafrost stability types from the 1960s to the 2000s in the QTP (%)

1960s / 2000s	Extremely stable	Stable	Sub-stable	Transitional	Unstable	Extremely unstable	Seasonally frozen ground
Extremely stable	24.75	0.78	0.00	0.00	0.00	0.00	0.00
Stable	59.42	9.67	1.33	0.02	0.00	0.00	0.00
Sub-stable	15.82	50.93	8.37	1.45	0.03	0.00	0.00
Transitional	0.00	35.91	23.18	6.16	0.57	0.00	0.00
Unstable	0.00	2.72	67.07	66.82	17.19	0.66	0.00
Extremely unstable	0.00	0.00	0.05	25.49	32.80	3.39	0.12
Seasonally frozen ground	0.00	0.00	0.00	0.06	49.40	95.95	99.88
Class changes	75.25	90.34	91.63	93.84	82.81	96.61	0.13

Table 5. The mean change in altitude of the permafrost thermal stability types over the QTP in the past 50 years (unit: metre)

Permafrost stability	1960s	1970s	1980s	1990s	2000s	Rate (m/decade)	R^2
Extremely stable	5240	5161	5169	5232	5328	24.7	0.34
Stable	5050	5052	5055	5094	5147	23.6	0.80
Sub-stable	4881	4932	4937	4985	5036	36.3	0.96
Transitional	4756	4799	4804	4859	4941	43.0	0.91
Unstable	4614	4670	4675	4713	4775	36.5	0.94
Extremely unstable	4392	4503	4513	4565	4642	56.2	0.94
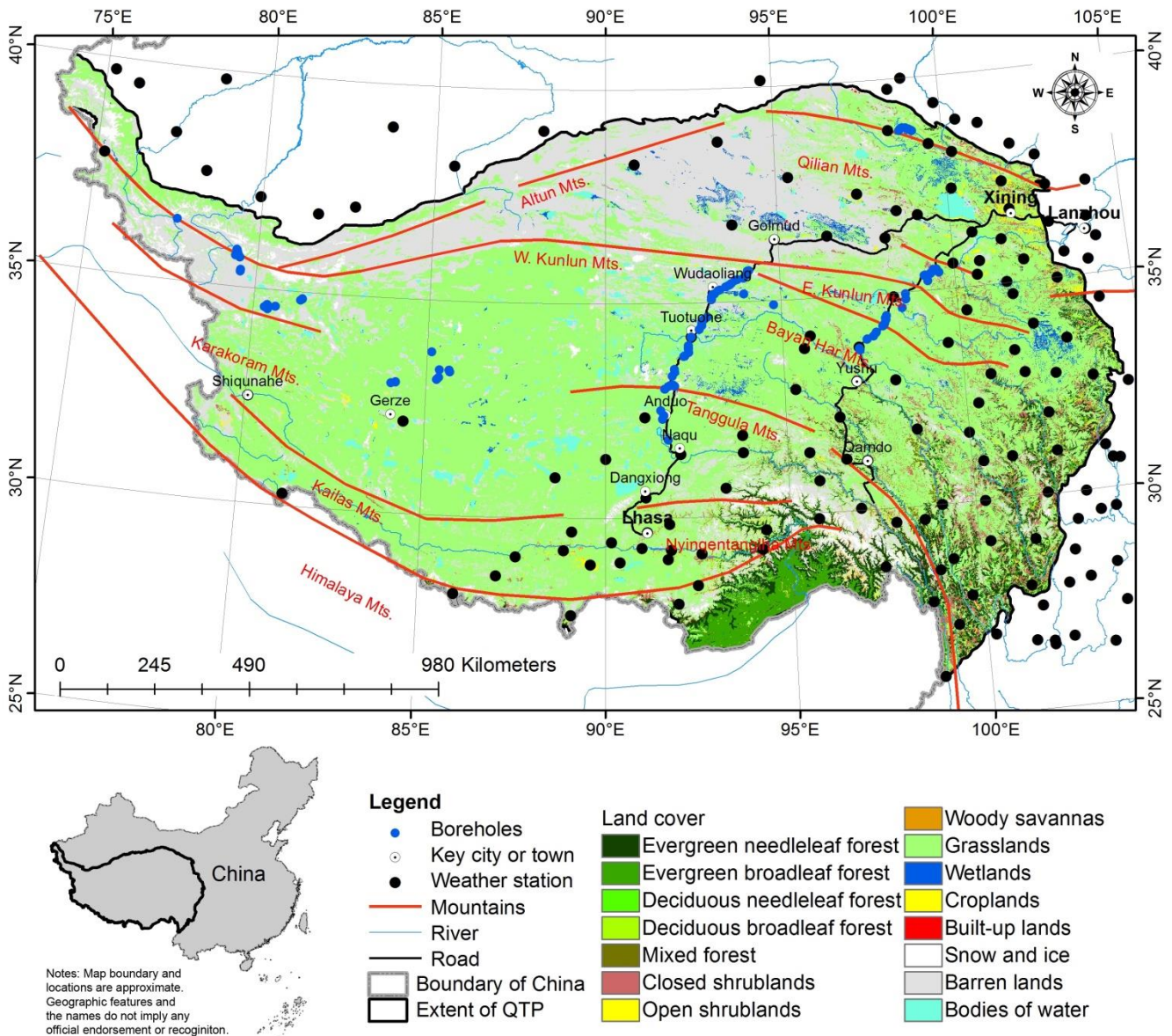
Figure 1. The distribution of in situ MAAT observation stations and MAGT boreholes over the QTP.

The Cryosphere
Discussions
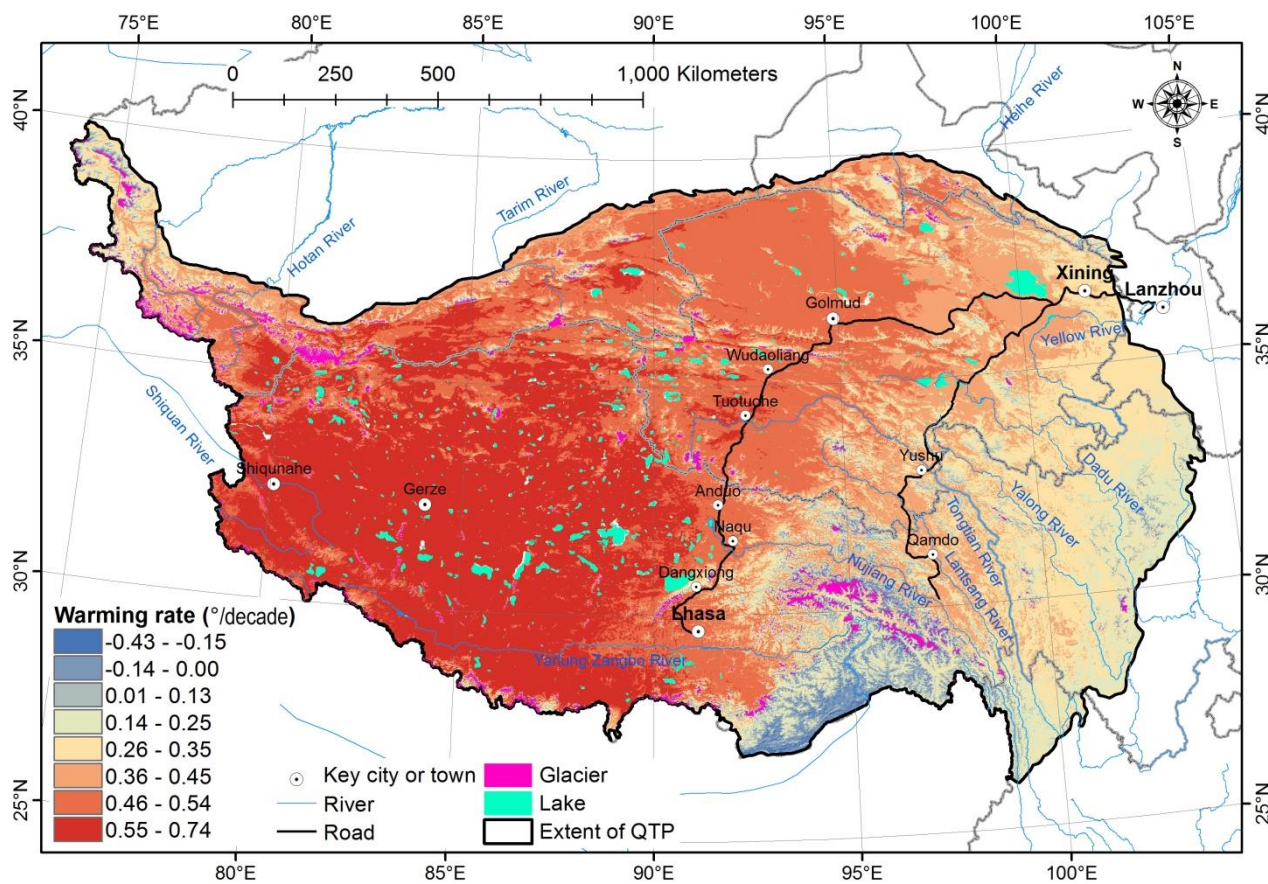
Figure 2. Spatial variability of MAAT warming rates over the QTP in the past 50 years.
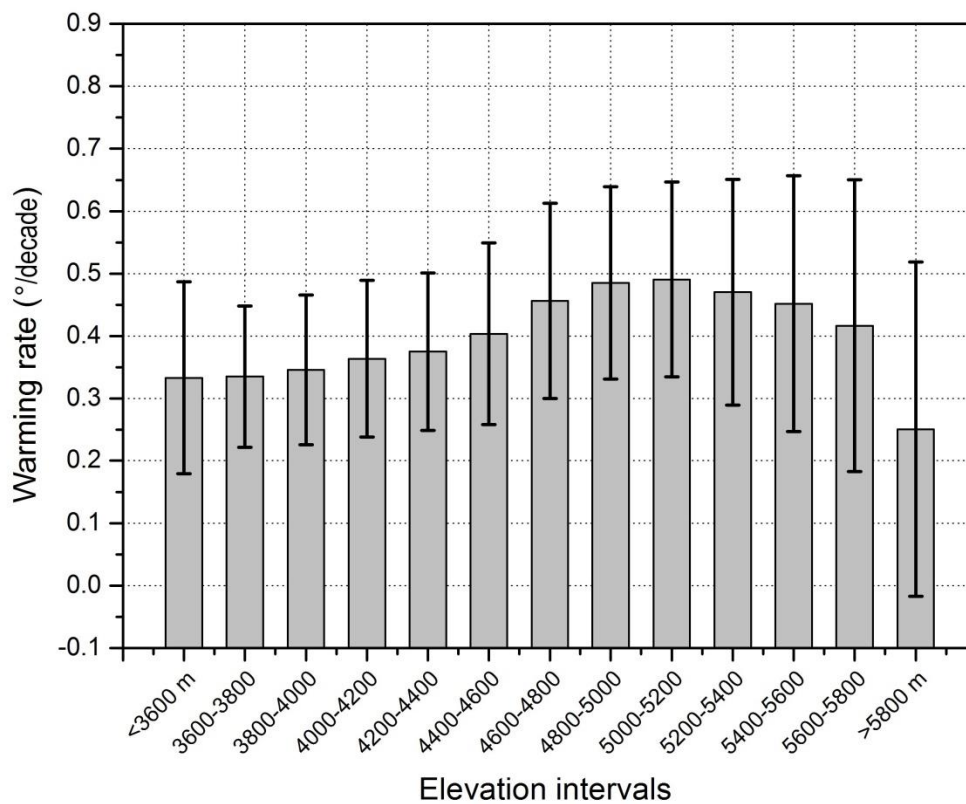
Figure 3. Warming rates with increasing elevation. These rates are derived from MAATs estimated using MODIS LSTs. Error bars display the standard deviations.
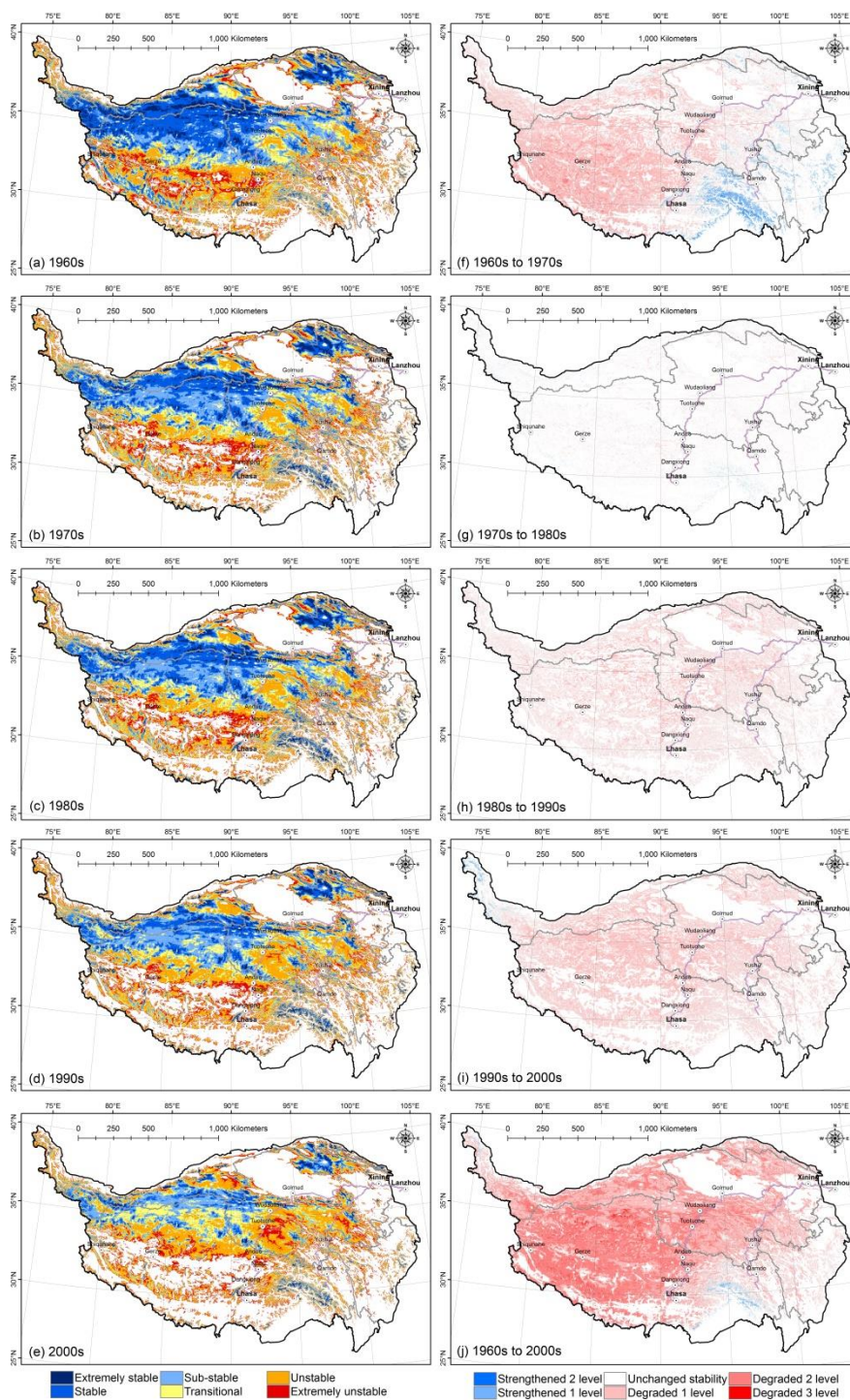
Figure 4. The permafrost stability map in each decade (a-e) and its spatial changes from the 1960s to the 2000s (f-j) over the QTP during the past 50 years.
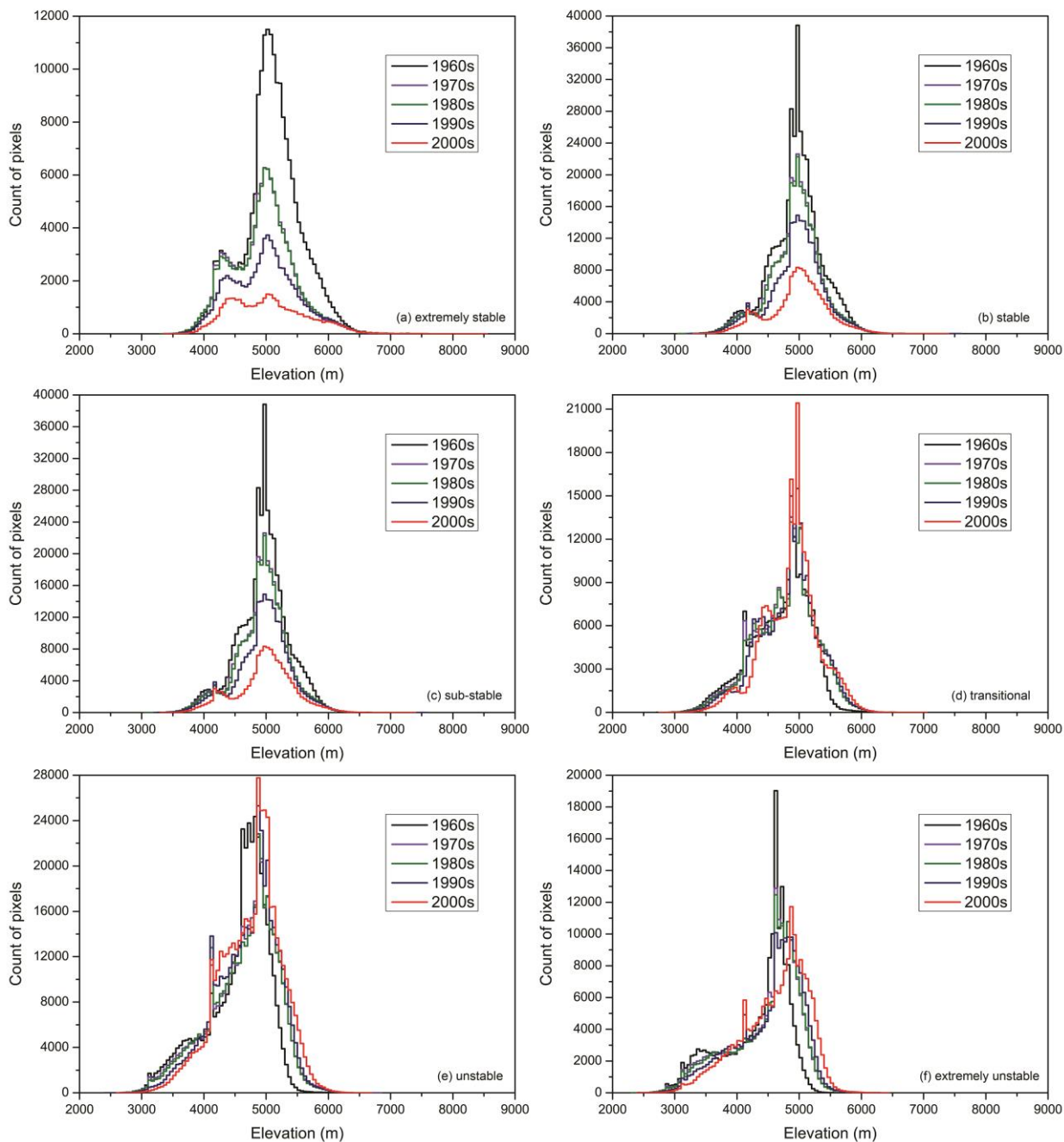
Figure 5. Changes in altitude distribution for extremely stable (a), stable (b), sub-stable (c), transitional (d), unstable (e), and extremely unstable (f) permafrost over the QTP in the past 50 years.
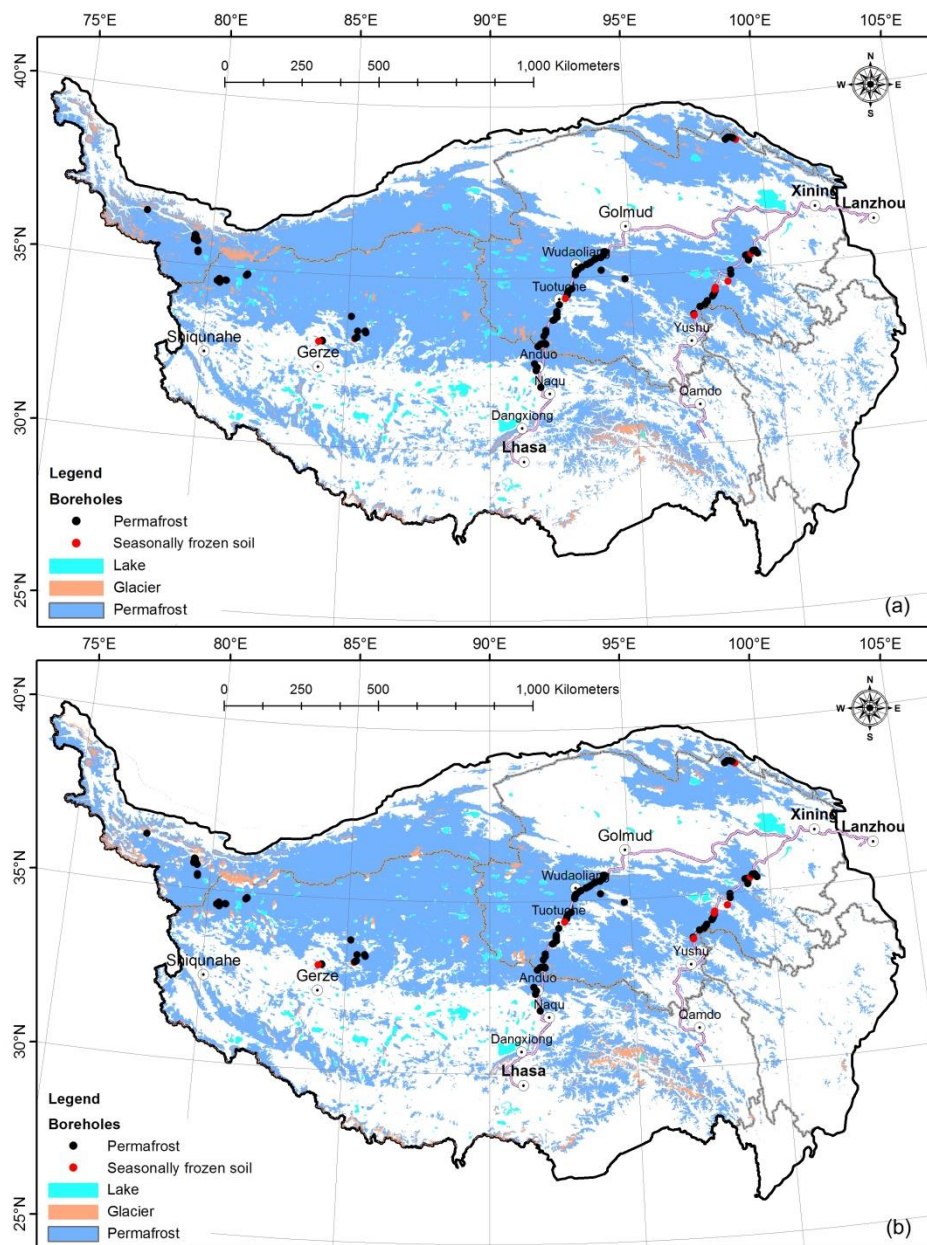
Figure 6. Comparison of the permafrost extent between the results of this study (a) and the new permafrost map (b).